Reduced Electron Recombination of Dye-sensitized Solar Cells based on TiO_2 Spheres Consisting of Untrathin Nanosheets with [001] facet exposed

Hongxia Wang,* Meinan Liu, Cheng Yan, John Bell

School of Engineering Systems, Queensland University of Technology, 2 George Street, GPO Box 2434, Brisbane, QLD 4001, Australia

Abstract:

An anatase TiO_2 material with hierarchical structured spheres consisting of untrathin nanosheets with 100% [001] facet exposed was employed to fabricate dye-sensitized solar cells (DSCs). Investigation of the electron transport and back reaction of the DSCs by electrochemical impedance spectroscopy showed that the spheres had a 3-fold lower electron recombination rate compared to the conventional TiO_2 nanoparticles. In contrast, the effective electron diffusion coefficient, D_n, was not sensitive to the variation of the TiO_2 morphology. The TiO_2 spheres showed the same D_n with that of the nanoparticles. The influence of $TiCl_4$ post-treatment on the conduction band of the TiO_2 spheres and on the kinetics of electron transport and back reactions was also investigated. It was found that the $TiCl_4$ post-treatment caused a downward shift of the TiO_2 conduction band edge by 30 meV. Meanwhile, a 4-fold increase of the effective electron lifetime of the DSC was also observed after $TiCl_4$ treatment. The synergistic effect of the variation of the TiO_2 conduction band and the electron recombination determined the open circuit voltage of the DSC.

Keywords: TiO_2 [001] facet, dye-sensitized solar cells, electron recombination, electrochemical impedance spectroscopy, untrathin nanosheet

Introduction

In the past two decades, dye-sensitized solar cells (DSCs) have received substantial attention from both academic and industrial communities as one of the most promising low cost, high efficiency third generation photovoltaic devices [1,2]. A typical DSC consists of a dye coated TiO_2 electrode

which is deposited on a fluorine doped tin oxide (FTO) conductive glass substrate, a I^-/I_3^- redox couple based electrolyte and a platinum counter electrode. Upon illumination, the photo with high energy (higher than the energy difference between the HOMO and LUMO level of the dye molecule) excite an electron from the ground state of the dye molecule to its excited state. The electron is then injected to the conduction band of the adjacent TiO_2 material owing to a favorable energetics alignment. The electron goes through a series of trapping/detrapping process in the TiO_2 film before reaching the current collector based on the fluorine doped tin oxide (FTO) conductive substrate. Meanwhile, a parallel reaction which involves transferring the hole from the oxidized state of the dye (dye^+) to the surrounding I^- ions of the redox couple of the electrolyte occurs to regenerate the dye molecule, resulting in the formation of I_3^- ions. The electrical circuit is completed through transferring the electron which arrives at the Pt counter electrode through external circuit to the I_3^- ions of the electrolyte.

Apparently, the operation of a DSC depends on several reactions which occur at the interface between different materials [3]. In particular, the process of electron injection at the interface of TiO_2/dye and the electron recombination reaction at the interface of TiO_2/dye/electrolyte are critical because they control both the short circuit current and open circuit voltage of the DSC. The surface property of the TiO_2 material plays an important role in both processes. The electron injection process in DSCs is controlled by the energy difference between the conduction band of TiO_2 material and the LUMO level of the dye, and the electron recombination process is mainly dominated by the interaction between the electron at the surface of TiO_2 and I_3^- ions in the electorlyte. Generally, the TiO_2 used in DSCs is based on anatase phase with [101] facet exposed due to the robust stability of this surface compared to other crystal facet [4]. It has been reported that the average surface energy of different facet of anatase TiO_2 has the order of [001] (0.90 J/m^2) > [100] (0.53 J/m^2) > [101] (0.44 J/m^2) [5]. Apparently, the lowest surface energy of [101] facet is the most stable surface in TiO_2 material. With the progress of synthesis technique, other active facets of TiO_2 crystals such as [001] which is normally unstable due to a higher surface energy can now be made however [6]. In practice, TiO_2 material with a large pecentage of [001] high energy surface has shown superior performance in

applications such as water splitting and lithium ion battery [6-8]. Further investigation shows that the [001] surface is beneficial to the photooxidization process through the O^- centres compared to the [101] surface which contains more Ti^{3+} centres [9].

The different surface property of the [001] and [101] facet of TiO_2 is expected to have profound effect on the chemicophysical processes in DSCs as well. Fan *et al* have reported that the [001] surface can absorb more dye molecules compared to the [101] surface [10]. However, the influence of TiO_2 [001] facet on the kinetics of electron transfer and back reaction has not been reported. A deep understanding of the role of TiO_2 [001] facet in these key processes of electron transport and recombination of DSCs is of great importance for both practical applications and basic research.

In this work, anatase TiO_2 spheres with a hierarchical structure consisting of untrathin nanosheets with 100% [001] facet exposed were synthesized and applied in dye-sensitized solar cells (DSCs). The photovoltaic performance of the DSCs with different concentration of the hierarchical structured TiO_2 spheres was evaluated. The kinetics of electron transport and back reaction of the DSCs with the spheres were investigated by electrochemical impedance spectroscopy. In addition, the effect of $TiCl_4$ aqueous solution treatment on the performance of the DSCs with the TiO_2 spheres was discussed.

Experimental

Synthesis of TiO_2 nanosheet particles

Hierarchical structured TiO_2 spheres of the nanosheets were synthesized by following the method which was originally reported by Chen *et al [6]*. Briefly, a precursor solution containing titanium isopropoxide (Sigma-Aldrich) (1.15 ml) and diethylenetriamine (DETA) (0.02 ml) in 32 ml isopropanol was prepared by magnetic-stirring the mixture of the three components vigorously at room temperature. The precursor solution was then transferred to a Teflon-lined stainless steel autoclave (45 ml volume, Parr Instrument Co.) for the hydrothermal reaction. The hydrothermal process was carried out at 200 ^oC for 24 h in an electric oven. After that, the autoclave was cooled to room temperature naturally. The as-collected white powder was washed with deionized water and

then ethanol for several times to remove the organic residues. The powder was then dried at 80^{o}C for 5 h and then sintered at 400 ^{o}C for 3 h to improve the crystallinity.

Fabrication of TiO_2 paste

TiO_2 pastes for the DSCs were fabricatd by mixing methylcellulose (Mw = 20,000), α-terpinol and the as-prepared TiO_2 powder with controlled amount using megnetic stirring at 80 ^{o}C for 48 h. Two sets of paste with different concentration of the TiO_2 powder were prepared. Paste A contained 13 wt% TiO_2 powder, 2.6 wt% methylcellulose and 84.4 wt% α-terpinol. Paste B contained 25 wt% TiO_2 powder, 2.5 wt% methylcellulose and 72.5 wt% α-terpinol. A commercial TiO_2 paste (DSL-18-NR, Dyesol) consisting of anatase TiO_2 nanoparticles with an average size of 20 nm was employed for comparison.

Assembly of dye-sensitized solar cells

The procedure for fabrication of the dye-sensitized solar cells has been reported in our previous work [11,12]. Briefly, a substrate based on fluorine doped tin oxide (FTO) conductive glass (TEC15, Pilkington) was thoroughly washed with detergent water, distilled water, acetone, isoproponal and ethanol in sequence under sonication for 15 mins. The cleaned FTO substrate was first coated with a compact layer of TiO_2 film by spray pyrolysis to reduce the electron back reaction at the interface of bare FTO and the electrolyte. The substrate was then deposited with the as-prepared TiO_2 paste or the commercial paste by a doctor-blading method using a Schotch tape as a spacer to control the thickness of the film. The TiO_2 film was dried on a hotplate at 90 ^{o}C for 10 mins before being sintered at 450 ^{o}C for 30 mins to form a mesoporous structure. The average thickness of the TiO_2 film was 13 μm. TiO_2 film with $TiCl_4$ post-treatment was carried out by immersing the sintered film in $TiCl_4$ aqueous solution (40 mM) at 70 ^{o}C for 30 mins. The film was washed with distilled water thoroughly and blow dried with N_2 gas. The film was then resintered at 450 ^{o}C for 30 mins. The geometrical area of the TiO_2 film was 0.25 cm^2.

The TiO_2 film (with or without $TiCl_4$ treatment) when it was still warm (around 80 ^{o}C) was immersed in a dye solution containing 0.25 mM *cis*-bis(isothiocyanato) bis(2,2'- bipyridyl-4,4'-dicarboxylate) ruthenium(II) bis-tetrabutylammonium (N719, Dyesol) in ethanol for 16 hours to form a dye coated

photoanode. A platinum counter electrode was prepared by dropping 5 μl isopropanol solution containing $H_2PtCl_6.6H_2O$ (5 mM) on a cleaned FTO substrate (1.5 ×1.0 cm^2). After dry in air, the substrate was then sintered at 390 ^oC for 15 mins in an electric oven to form a thin Pt layer on the FTO substrate. A dye-sensitized solar cell was assembled by sealing the dye coated TiO_2 electrode with the platinized FTO counter electrode using a thermal plastics (Surlyn 1705) at 130 ^oC. The electrolyte composed of 0.6 M 1-propyl-3-methylimidiazolium iodide, 0.05 M I_2, 0.1 M guanidinium thiocyanate, 0.2 M NaI, 0.1 M N-methyl benzimidazole in 3-methoxypropionitrile was introduced into the space between the electrodes through the holes which were predrilled in the Pt counter electrode by a vacuum-assisted technique. The holes were then sealed using a Surlyn film covered with a microscope slip.

Characterization

The morphology and the crystal structure of the as-prepared TiO_2 powder were investigated by scanning electron microscope (SEM, FEI Quanta 200) and powder X-ray diffraction (XRD, PANanalytical Xpert Pro), respectively. Transmission electron microscopy (TEM, Philips CM 200) was used to monitor the detailed structure of the TiO_2 powder. The thickness of the TiO_2 films for the DSCs was determined by a profilometer (Dektak 150). The photocurrent density-voltage (*J-V*) characteristics of the DSCs was obtained using a Xe lamp (150 W) based solar simulator (Newport) by recording the current of the cells as a function of the applied bias under AM1.5 illumination (100 mW/cm^2) with a computer-controlled digital source meter (Keithley 2420). The illumination intensity of the incident light from the solar simulator was measured with a silicon photodiode which was calibrated with an optical meter (1918-C, Oriel). Aluminum foil with size comparable to the active area of the TiO_2 film was used as reflector on the counter electrode side of the DSCs during the *J-V* measurement.

The electrochemical impedance spectroscopy (EIS) of the DSCs was measured in the frequency range of 50,000 - 0.1 Hz at room temperature by a Versa-stat 3 electrochemical workstation (Princeton Applied Research). The EIS measurement was carried out under illumination which was provided by

a light emitting diode (LED, 627 nm) at open-circuit. The intensity of the incident illumination on the front side of the DSC (TiO_2 side) was adjusted using a combination of neutral density filters. The EIS spectrum was analysed with a Zview software using a transmission line based equivalent circuit to obtain the information of chemical capacitance, electron recombination resistance and electron transport resistance of the DSCs [12,13].

3. Results and discussions

Figure 1(a) shows the image of the as-prepared TiO_2 powder by SEM. The material consists of micro-sized particles with sphere shape. The surface of the sphere is very rough and seems fluffy. The diameter of the sphere is around 1.6 μm as determined by TEM (Figure 1b). TEM images (Figure 1b and c) also illustrate that the sphere has sub-structure which is consisting of untrathin nanosheets that are packed together. It is spculated that the sphere is formed through self-assembly of the nanosheets to realize a minimum surface energy. Some spheres have pits on the surface which may be due to the insufficient reaction duration. The measurement of the N_2 adsorption/ desorption isotherms of the TiO_2 powder shows that the specific surface area of the TiO_2 spheres is 82 m^2/g, which is slightly higher than the specific surface area of the film made from the commercial TiO_2 paste (DSL-18NR, Dyesol. Surface area: 72.9 m^2/g) [14]. The large surface area of the material suggests that the nanosheets are probably loosely packed so that more suraface areas are exposed. The XRD pattern of the material (Figure 1(d)) shows that the as-prepared TiO_2 powder is anatase with a tetragonal structure and space group *I*41*/amd* (JCPDS card, No. 71-1169). Both the TEM images and the XRD results are in good agreement with the results reported by Chen *et al*. According to Chen *et al*, the TiO_2 spheres synthesized by this method have 100% [001] surface exposed [6].

The SEM image of the TiO_2 film consisting of the spheres is shown in Figure 1(e) and Figure 1(f). Apparently, the TiO_2 particles are connected with each other in the film. Figure 1(f) shows that the film contains large amount of small pores. However, the sphere of the TiO_2 particles is rarely seen in the film. This indicates that the mechanical force of grinding and sonication employed in the preparation of the film broke up the spheres into small particles, probably in the form of nanosheets.

Nevertheless, the same XRD pattern of the sintered TiO_2 film (not shown) indicates that the film has the same surface property with the spheres.

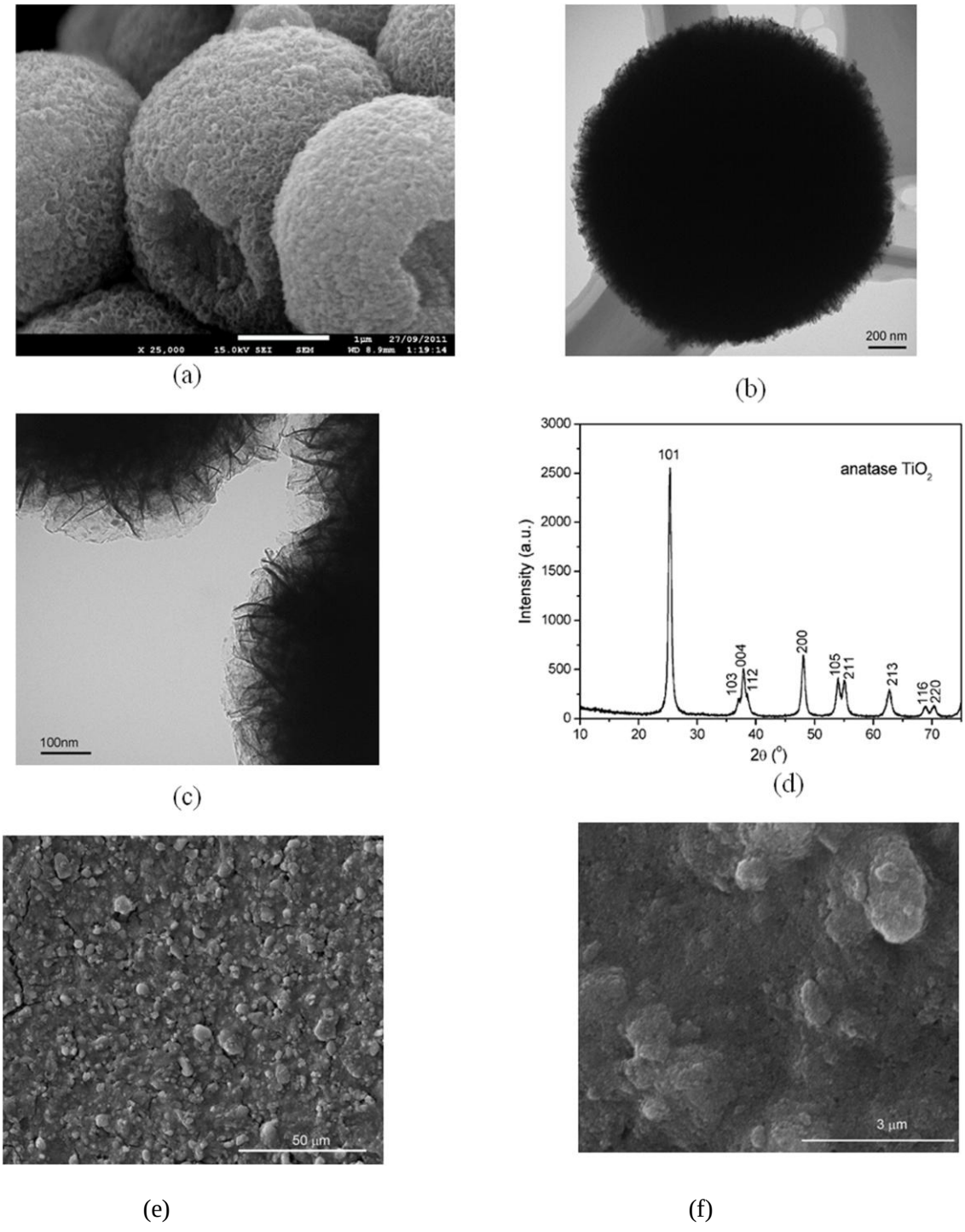

Figure 1. Images of TiO_2 particles by SEM (a) and by TEM (b, c) as well as XRD pattern of the TiO_2 particles (d) and morphology of the TiO_2 film consisting of the as-prepared sphere particles (e, f).

J-V characteristics of the DSCs

The *J-V* characteristics of the DSCs with the TiO_2 film made from paste A which contained 13 wt% TiO_2 spheres with and without $TiCl_4$ post-treatment is shown in Figure 2(a). The DSC solely based on paste A without $TiCl_4$ treatment (Curve A) produced a short circuit current density (J_{sc}) of 8.79 mA/cm^2 and open circuit voltage (V_{oc}) of 0.76 V. In contrast, when the TiO_2 film was subject to $TiCl_4$ solution treatment, the J_{sc} of the DSC (curve B) is increased to12.1 mA/cm^2, which is 37.5% higher than that of Curve A.

Figure 2(b) shows the *J-V* performance of the DSCs made from Paste B which contains 25 wt% as-prepared TiO_2 nanosheet based particles. The J_{sc} of the cell is 15.6 mA/cm^2 and V_{oc} = 0.70 V (Figure 2(b), Curve C) when there was no $TiCl_4$ treatment. Compared to Curve A, it is found that the ratio of the J_{sc} of Curve C to that of Curve A ((15.6 mA/cm^2)/(12.1 mA/cm^2) = 1.77) is very close to the ratio of the concentration of the TiO_2 spheres in the two pastes ((TiO_2 wt% in paste B)/(TiO_2 wt% in paste A) = (25)/(13) = 1.92). It suggests that the higher J_{sc} of the DSC made from Paste B is due to the availability of more TiO_2 particles in the film which can absorb more dye molecules, leading to a higher light absorption. The J_{sc} of the DSC made from Paste B is further increased from 15.6 mA/cm^2 (Figure 2(b), Curve C) to 18.2 mA/cm^2 when the TiO_2 film was processed with $TiCl_4$ solution (Figure 2(b), Curve D). Meanwhile, the V_{oc} of Curve D is 20 mV higher than that of Curve C, suggesting the beneficial effect of $TiCl_4$ post-treatment on V_{oc} as well. The best performance is obtained with curve D with power conversion efficiency = 7.57% (Figure 2(b)), which is comparable to the efficiency (η= 7.52%) of the DSCs (I-V curve is not shown) made from the commercial paste. The detailed characteristic parameters of the performacne of the DSCs with different TiO_2 pastes are shown in Table 1.

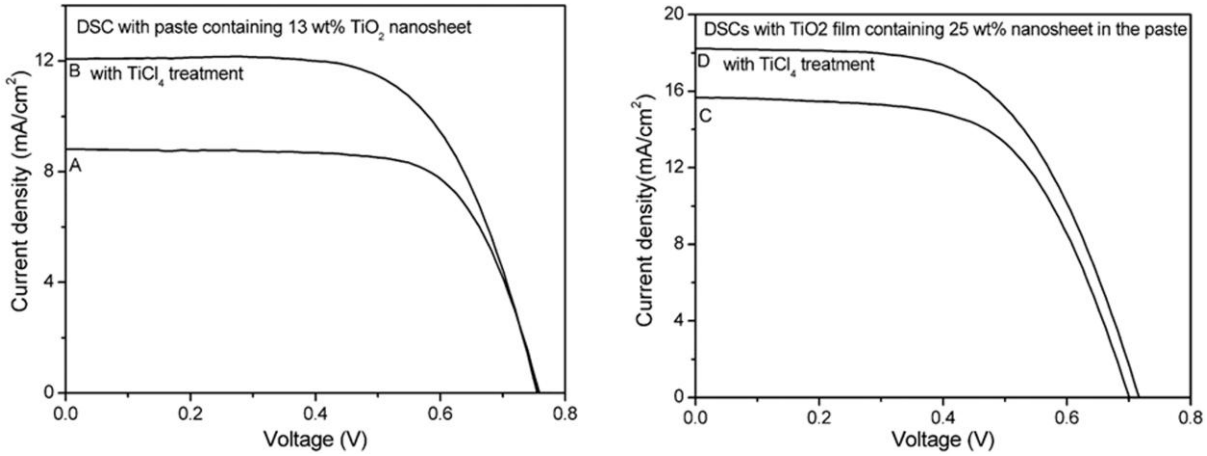

(a) (b)

Figure 2: *J-V* characteristics of the dye-sensitized solar cells made from Paste A containing 13 wt% TiO_2 spheres (a) and from Paste B containing 25 wt% spheres (b) with (Curve B and D) and without (Curve A and C) $TiCl_4$ treatment

Table 1. Characteristic performance parameters of the dye-sensitized solar cells

Cell name	J_{sc} **(mA/cm^2)**	V_{oc} **(V)**	***FF***	**Efficiency (%)**
13 wt%TiO_2 nanosheet (Curve A)	8.79	0.757	0.7	4.66
13 wt% TiO_2 nanosheet with $TiCl_4$ treatment (Curve B)	12.07	0.754	0.646	5.88
25wt% TiO_2 nanosheet (Curve C)	15.6	0.7	0.61	6.66
25wt%TiO_2 nanosheet with $TiCl_4$ treatment (Curve D)	18.2	0.72	0.58	7.57
DSC made from TiO_2 nanoparticles	16.5	0.755	0.604	7.52

Electrochemical Impedance spectroscopy

The information on the charge transfer and transport process in DSCs can be measured by small perturbation based transient methods such as electrochemical impedance spectroscopy (EIS) or intensity modulated photocurrent spectroscopy (IMPS) and intensity modulated photovoltage spectroscopy (IMVS) [13,15]. Compared to IMPS and IMVS, the advantage of EIS method for

characterization of DSCs lies in that both the effective electron lifetime, τ_n, and the effective electron diffusion coefficient, D_n, can be obtained in one measurement. This is achieved by fitting the EIS spectrum using a suitable equivalent circuit that mimicks the physical process in the device. The equivalent circuit which depicts the process of electron trapping/detrapping in DSCs is shown in Figure 3(a). It contains a series resistance, R_s, a capacitance at Pt elctrode/electrolyte interface, C_{Pt}, and a resistance for the charge transfer process between electrons at Pt electrode and I_3^- ions of the electrolyte, R_{Pt}. Z_w is the Warburg resistance arising from the ion transport in the electrolyte and Z_{tl} is a distribution line describing the electron transport and recombination in the mesoporous TiO_2 film [13,16]. A typical EIS spectrum of a DSC is shown in Figure 3(b) for the Nyquist plot and Figure 3(c) for the Bode plot. The corresponding fitting results (green line) using the equivalent circuit are also shown in Figure 3 (b, c). The distorted semicircle in the high frequency range (above 10 Hz) is ascribed to the electron transfer process at the interface of Pt counter electrode/electrolyte combined with the electron transport process in the TiO_2 film (the semicircle corresponding to the electron transport process in TiO_2 is buried in the semicircle of the charge transfer process at Pt/electrolyte interface in the spectrum) [3]. The large semicircle in the lower frequency range (10 - 0.1 Hz) is due to the electron recombination process in the TiO_2 film. Under a high incident illumination intensity, the density of the photo-generated electron in the TiO_2 film is very high (up to $10^{18}/cm^3$) and the TiO_2 film becomes conductive [17]. In this case, the resistance corresponding to the electron transport process becomes too small to be observed in the EIS spectrum. Consequently, the EIS spectrum is mainly dominated by the electron recombination process. Nevertheless, under a low incident illumination intensity, the conductivity of the TiO_2 film is very low due to a low density of the photo-generated electron. In this case, the main feature of the EIS spectrum is due to the transport of electron in the TiO_2 film. Hence, an accurate fitting of the EIS spectrum of a DSC using the equivalent circuit is normally obtained in the illumination range when both the electron transport resistance and the electron recombination resistance are substantial [13]. Only the results from good fittings are shown in this work.

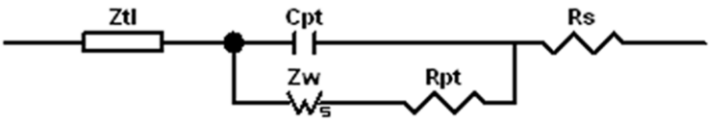

(a)

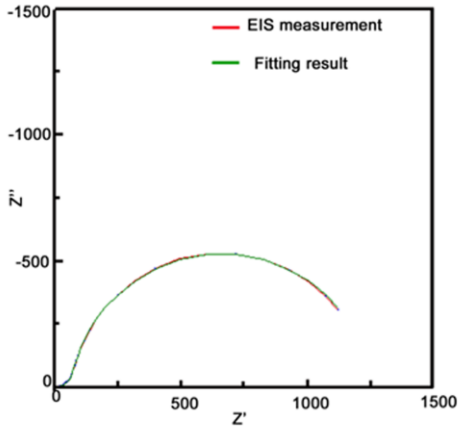

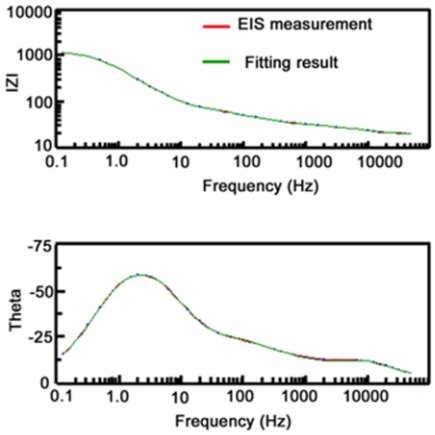

(b) (c)

Figure 3. Equivalent circuit (a) and the Nyquist plot (b) and Bode plot (c) of the impedance spectrum of a dye-sensitized solar cell

Comparison of electron transport and recombination of the DSC based on TiO_2 spheres and nanoparticles

The electron recombination process in DSCs is reflected by the effective electron lifetime, τ_n whereas the electron transport process is manfested by the effective electron diffusion coefficient D_n. Bisquert *et al* have shown that both τ_n and D_n of a DSC are dependent on the distribution of density of electron in the conduction band (free electron) and in the trap states (trapped electron) of the TiO_2 film as well as the lifetime and diffusion coefficient of free electron (τ_0 and D_0) through the following consideration

$$\tau_n = \left(1 + \frac{\partial n_t}{\partial n_c}\right)\tau_0 \qquad \text{(Eq.1)}$$

and $$D_n = \left(1 + \frac{\partial n_t}{\partial n_c}\right)^{-1} D_0 \qquad \text{(Eq.2)}$$

where n_t and n_c are the density of the trapped electron and free electron respectively [18].

The charge distribution, g(E), in a mesoporous TiO_2 film is described by [18,19]:

$$g({}_nE_F) = \frac{N_{t,0}}{k_B T_0} \exp(-\frac{E_c - {}_nE_F}{k_B T_0}) = \frac{N_{t,0}}{k_B T_0} \exp(-\frac{E_c - E_{F,redox} - qV}{k_B T_0}) \quad \text{(Eq.3)}$$

Where ${}_nE_F$ is the quasi-Fermi level of TiO_2, E_c the conduction band of TiO_2, and $E_{F,redox}$ the potential energy of the redox couple, $N_{t,0}$ the total density of the trapped electron, k_B is the Boltzmann constant and T_0 the characteristic temperature which reflects the profile of the charge distribution in TiO_2.

Therefore, comparison of the change of τ_n and D_n in DSCs due to the different material component should be made by using density of charge as the reference provided that the distribution profile of charge density is the same[20].

Because the density of charge in the TiO_2 film is reflected by the chemical capacitance, C_μ, which is measured by EIS, through the relationship [18]:

$$C_\mu({}_nE_F) = \int_{E_v}^{E_c} C_\mu({}_nE_F, E)dE \approx q^2 g({}_nE_F) \quad \text{(Eq.4)}$$

We employ density of chemical capacitance as the reference for the investigation of the variation of τ_n and D_n in the following.

Figure 4(a) shows the τ_n of the DSCs with the TiO_2 films consisting of the nanosheets based spheres and the conventional nanoparticles as a function of the chemical capacitance density. It is found the τ_n of the nanosheets based DSC is nearly 3-fold higher than that of the nanoparticles for a constant capacitance density. It suggests that the TiO_2 film with the spheres has a lower electron recombination reaction rate compared to the film with the nanoparticles. Besides τ_n, the effective electron diffusion coefficient, D_n, is another important parameter which controls the performance of a DSC. The comparison of the D_n of the cell based on the spheres and the nanoparticles is shown in Figure 4(b). It is interesting that both materials show the same D_n, suggesting that the electron transport is not affected by the morphology and the exposed crystal facet of TiO_2 material. The identical D_n also suggests that the diffusion coefficient of the free electron is the same for the two materials according to Eq.2 [13]. It also justifies the assumption that the profile of the distribution of charge density is the same in the two types of TiO_2 film. In constrast, the different τ_n suggests that the free electron

lifetime of the spheres is different from that of the nanoparticles. The low τ_n of the spheres could be related with the property of the [001] facet, but clarification of this issue needs more investigations. As a consequence, the electron diffusion lengh, L_n, which depends on both the τ_n and D_n by $L_n = \sqrt{t_n D_n}$, is up to 1.6-fold higher for the nanosheet based TiO_2 spheres than that of the nanoparticles (Figure 4(c)). It is found that the L_n of the DSC based on the nanoparticles is only around 16 μm (Figure 4(c)), which is comparable to the thickness of the TiO_2 film (13 μm). Previous study has shown that the L_n of a DSC needs to be at least 3-fold the thickness of the TiO_2 film in order to collect most of the photogenerated electrons [13]. Therefore, the short L_n may limit the performance of the DSC. The higher L_n of the spheres based DSC should benefit a higher electron collection efficiency compared to the nanoparticles counterpart.

Besides J_{sc}, V_{oc} is another key performance parameter of a DSC. The maximum voltage of a DSC is determined by the potential difference between the conduction band of TiO_2 and the redox potential of I^-/I_3^- in the electrolyte. Obviousy, the position of the TiO_2 conduction band edge, E_c, has direct impact on the open circuit voltage (V_{oc}) of the DSC. Thus it is important to know the relative position of the E_c of the nanosheets based spheres relative to the nanoparticles in order to disclose the reason for the different V_{oc}. According to Equation 3, the change of E_c of TiO_2 can be monitored by the variation of the voltage (V) of the DSC at a constant electron density.

As shown in Figure 4(d), the E_c of the nanosheet based spheres is found to be 100 meV lower than that of the nanoparticles. The lower E_c of the spheres is probably due to the different dye uploading on the TiO_2 films. According to Fan *et al [10]*, TiO_2 [001] facet can absorb more dyes than the [101] facet. Nazeeruddin *et al* have confirmed that the dye molecule is adsorbed on TiO_2 particles mainly through the carboxy acid group (–COOH) [4], leading to the protonation of the surface of TiO_2 and the downward shift of the E_c. The more dye molecules are adsorbed on the TiO_2 film, the more downward shift is expected for the E_c.

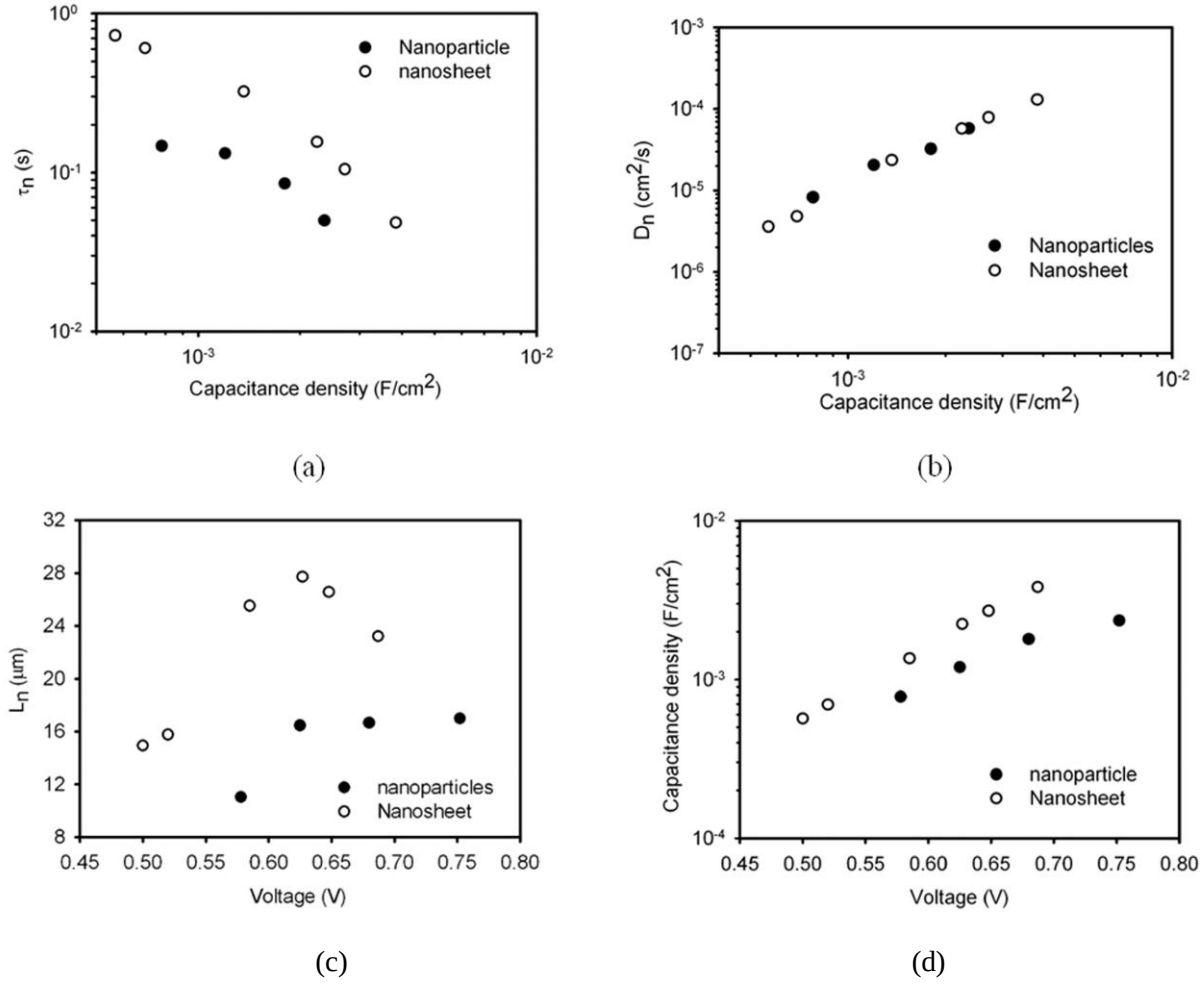

Figure 4. Comparison of the effective electron lifetime, τ_n, (a) and effective electron diffusion coefficient, D_n, (b) and electron diffusion length, L_n, (c) of the DSCs with TiO_2 nanosheets (open circle) and with conventional nanoparticles(solid circle). (d) Variation of the chemical capacitance density of the nanosheets and nanoparticles as a funcion of voltage.

Effect of $TiCl_4$ treatment

The strategy of treating TiO_2 mesoporous film with $TiCl_4$ aqueous solution has extensively been employed to improve the performance of DSCs. In most cases, it is found that the J_{sc} of the DSC is enhanced while the V_{oc} is reduced after the $TiCl_4$ treatment of the film. O'Regan *et al* found that $TiCl_4$ treatment caused 80 meV downward shift of the TiO_2 conduction band, resulting in an increased driving force for the electron injection process. They reported that the enhanced J_{sc} was owing to an improved electron injection efficiency of the DSC [21,22]. In the following section, the influence of

the $TiCl_4$ solution treatment on the E_c of the TiO_2 spheres based film and on the kinetics of electron transport and back reaction of the corresponding DSCs is investigated.

Figure 5 (a) illustrates the chemical capacitance density as a function of the voltage of the DSCs made from paste B with and without $TiCl_4$ treatment. It is found that, at a constant charge density, the voltage of the cell with $TiCl_4$ treatment is lower than that of the DSC without the treatment. The maximum difference in voltage between the cells is around 30 mV. Provided that the discribution profile of the charge density is the same of the TiO_2 film with and without $TiCl_4$ treatment, the reduced potential of the DSC with $TiCl_4$ treatment means that the $TiCl_4$ treatment caused a downward-shift of the TiO_2 conduction band by 30 meV, which may decrease the maximum voltage the DSC can achieve. This observation is in good agreement with the results reported by O'Regan *et al [21]*. However, the V_{oc} of the cell with $TiCl_4$ treatment is actually 20 mV higher than the DSC without the treatment as shown in Figure 2(b). This indicates that the electron recombination of the DSC is probably affected by the $TiCl_4$ treatment.

Figure 5(b) shows the τ_n as a function of capacitance density of the DSC with and without $TiCl_4$ treatment. It is found that τ_n is enhanced by 3.8-fold after $TiCl_4$ treatment. In contrast, D_n of the DSCs is relatively unchanged with the $TiCl_4$ treatment (Figure 5(c)). Owing to the enhanced τ_n, the electron diffusion length, L_n, of the DSC is enhanced by two-fold through $TiCl_4$ treatment (Figure 5(d)). Hence, the improved voltage (20 mV) of the DSC (Figure 2(b), curve D) with $TiCl_4$ treatment compared to the cell without $TiCl_4$ treatment (curve C in Figure 2(b)) should be a result of the synergistic effect of the decreased TiO_2 conduction band and the increased electron lifetime. Apparently, the beneficial effect of the enhanced electron lifetime on V_{oc} surpasses the negative effect of the downward-shift of the E_c of TiO_2, leading to a higher V_{oc}.

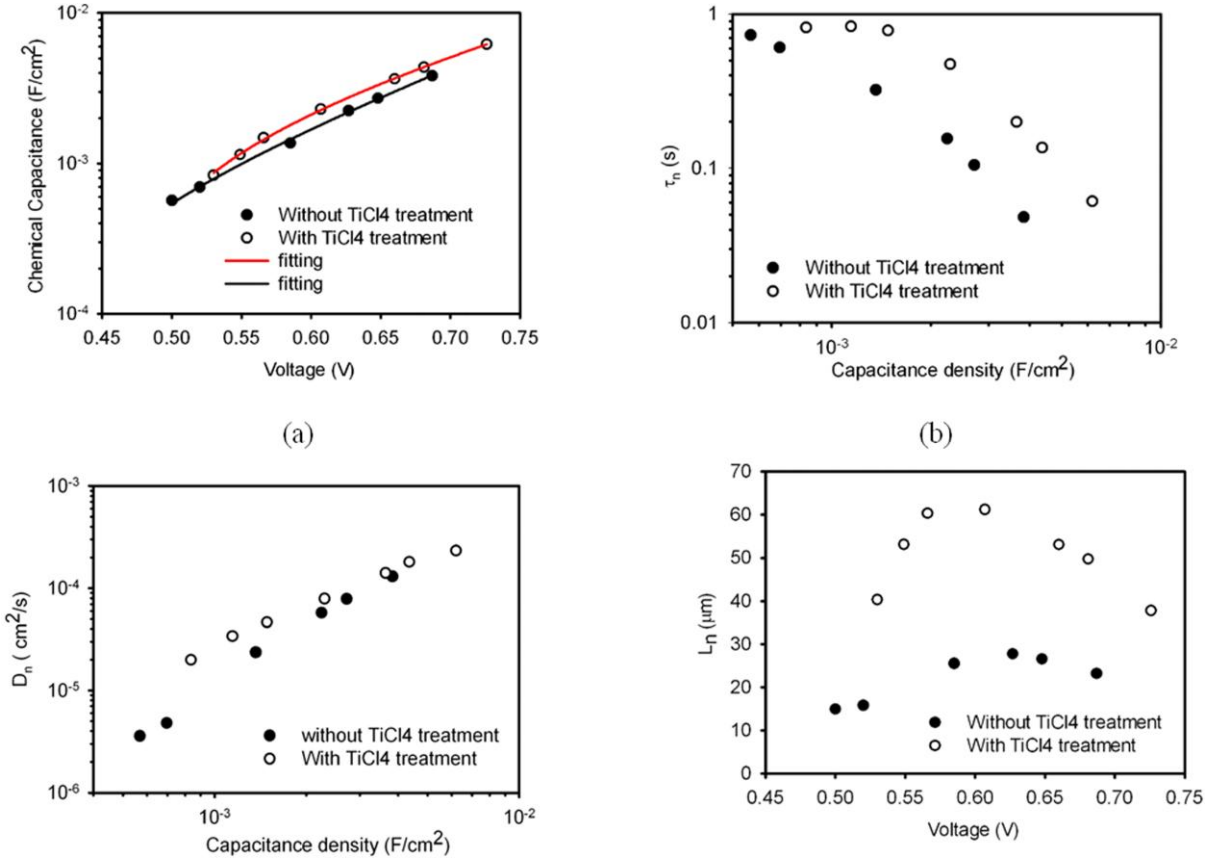

Figure 5. Comparison of dye-sensitized solar cells based on hierarchical structured TiO_2 spheres with and without $TiCl_4$ post-treatment. (a): chemical capacitance *vs* Voltage; (b): effective electron lifetime, τ_n, as a function of charge density; (c): effective electron diffusion coefficient, D_n, as a function of charge density; and (d): electron diffusion length, L_n as a function of voltage

Conclusion

Dye-sensitized solar cells with TiO_2 electrode made from hierarchical structured TiO_2 spheres consisting of nanosheets with 100% [001] facet exposed were assembled and characterized in terms of the device performance, the kinetics of electron transport and back reaction. It was found that the TiO_2 spheres based DSCs generated an energy conversion efficiency of 7.57%,which is comparable to the conventional TiO_2 nanoparticles. Investigation of the kinetics of electron transport and back raction of the DSCs showed that the spheres had a 3-fold higher effective electron lifetime compared to the

nanoparticles. However, the effective electron diffusion coefficient, D_n, of the DSCs was not affected by the different morphology and crystal facets exposed of the TiO_2 material. Monitor the variation of the conduction band of the dyed TiO_2 film disclosed that the E_c of the spheres based TiO_2 electrode was 100 meV lower than that of the nanoparticles.

This work also investigated the influence of $TiCl_4$ aqueous solution treatment on the E_c of the TiO_2 spheres and on the τ_n and D_n of the corresponding DSCs. It was found that $TiCl_4$ treatment caused a downward shift (30 meV) of the TiO_2 conduction band and four-fold increase of the τ_n whereas the D_n of the cell was not significantly affected by $TiCl_4$ treatment.

Acknowledgements

The authors (H. Wang and M. Liu) acknowledge the financial support by Queensland University of Technology *via* Vice-Chancellor Research Fellowship scheme.

References

1. Oregan, B.; Grätzel, M., A Low-Cost. *Nature* **1991**, 353, 737-740.

2. Wang, H. X.; Li, H.; Xue, B. F.; Wang, Z. X.; Meng, Q. B.; Chen, L. Q. *J. Am. Chem. Soc.* **2005**, 127 (17), 6394-6401.

3. Wang, H. X.; Bell, J.; Desilvestro, J.; Bertoz, M.; Evans, G.. *J. Phys. Chem. C* **2007**, 111 (41), 15125-15131.

4. Nazeeruddin, M. K.; Humphry-Baker, R.; Liska, P.; Grätzel, M. *J. Phys. Chem. B* **2003**, 107 (34), 8981-8987.

5. Liu, M.; Chang, J.; Yan, C., Bell. J.. *Int. J. Smart and Nano Mater.,iFirst*, **2011**, 1-9.

6. Chen, J. S.; Tan, Y. L.; Li, C. M.; Cheah, Y. L.; Luan, D. Y.; Madhavi, S.; Boey, F. Y. C.; Archer, L. A.; Lou, X. W. *J. Am. Chem. Soc.* **2010**, 132 (17), 6124-6130.

7. Yang, H. G.; Sun, C. H.; Qiao, S. Z.; Zou, J.; Liu, G.; Smith, S. C.; Cheng, H. M.; Lu, G. Q. *Nature* **2008**, 453 (7195), 638-642.

8. Zhu, J. A.; Wang, S. H.; Bian, Z. F.; Xie, S. H.; Cai, C. L.; Wang, J. G.; Yang, H. G.; Li, H. X. *Crystengcomm* **2010**, 12 (7), 2219-2224.

9. D'Arienzo, M.; Carbajo, J.; Bahamonde, A.; Crippa, M.; Polizzi, S.; Scotti, R.; Wahba, L.; Morazzoni, F.. *J. Am. Chem. Soc.* **2011**, 133 (44), 17652-17661.

10. Fan, J. J.; Cai, W. Q.; Yu, J. G. *Chemistry-an Asian Journal* **2011**, 6 (9), 2481-2490.

11. Wang, H. X.; Liu, M. N.; Zhang, M.; Wang, P.; Miura, H.; Cheng, Y.; Bell, J. *Phys. Chem. Chem. Phys.* **2011**, 13 (38), 17359-17366.

12. Villanueva-Cab, J.; Wang, H. X.; Oskam, G.; Peter, L. M. *J. Phys. Chem. Lett.* **2010**, 1 (4), 748-751.

13. Wang, H.; Peter, L. M. *J. Phys. Chem. C* **2009**, 18125-18131.

14. Samadpour, M.; Gimènez, S.; Zad, A. I.; Taghavinia, N.; Mora-Sero, I. *Phys. Chem. Chem. Phys*., 2012, 14, 522-528.

15. Bisquert, J. *J. Phys. Chem. B* **2002**, 106 (2), 325-333.

16. Wang, H.X.; Nicholson, P. G.; Peter, L.M.; Zakeeruddin, S. M.; Grätzel M. J. Phys. Chem. C 2010, 114, 14300-14306.

17. Nguyen, T. T. O.; Peter, L. M.; Wang, H. X. *J. Phys. Chem. C* **2009**, 113 (19), 8532-8536.

18. Bisquert, J., Vikhrenko, V.S. *J. Phys. Chem. B* 2004, 108, 2313-2322.

19. Peter, L. M. *J. Phys. Chem. C* **2007**, 111 (18), 6601-6612.

20. Wang, H. X.; Peter, L.M. *J. Phys. Chem.C 2012*, Accepted (**DOI:** 10.1021/jp211807w).

21. O'Regan, B. C.; Durrant, J. R.; Sommeling, P. M.; Bakker, N. J. *J. Phys. Chem. C* **2007**, 111 (37), 14001-14010.

22. Sommeling, P. M.; O'Regan, B. C.; Haswell, R. R.; Smit, H. J. P.; Bakker, N. J.; Smits, J. J. T.; Kroon, J. M.; van Roosmalen, J. A. M.. *J. Phys. Chem. B* **2006**, *110* (39), 19191-19197.